The Quantitative Proteomics Analysis in Glioblastoma After HULC Silencing

Shan Ye
Anhui Provincial Hospital Affiliated to Anhui Medical University
Yiran Wang
Anhui Provincial Hospital Affiliated to Anhui Medical University
Tiantian Yin
Anhui Provincial Hospital Affiliated to Anhui Medical University
Yuchen Hu
Anhui Provincial Hospital Affiliated to Anhui Medical University
Jie He (hejie23@ustc.edu.cn)
The First Affiliated Hospital of USTC

Research

Keywords: glioblastoma, HULC, proteomics, PLA2G4A

Posted Date: June 16th, 2020

DOI: https://doi.org/10.21203/rs.3.rs-33521/v1

Abstract

Background: Glioblastoma multiforme (GBM) is a malignant intracranial tumor threatening patients' survival. The study aimed to find the menchanisms of lncRNA highly up-regulated in liver cancer (HULC) affecting GBM or involved signaling pathways, which may providing theoretical support for targeted therapy.

Methods: Two cell lines were constructed: HULC-small interfering RNA (siRNA) and negative control. Then qRT-PCR was operated to detect the transfection efficiency and quantitative proteomics based on mass spectrometry (MS) were conducted. Finally, the differentially expressed proteins were analyzed in gene ontology (GO) classification and Kyoto Encyclopedia of Genes and Genomes (KEGG) pathway enrichment.

Results: The relative expression level of HULC in HULC-siRNA was significantly lower than that in NC detected by qRT-PCR. A total of 136 differentially expressed proteins were identified, including 24 down-regulated and 112 up-regulated. GO classification results illustrated that they were centralized in cellular or single-organism process and biological regulation in biological process, cell and organelle in cellular component, binding and catalytic activity in molecular function. KEGG pathway enrichment analysis indicated that some were sinificantly enriched, including tight junction, metabolic pathways and arachidonic acid metabolism. It was further discovered that PLA2G4A was down regulated obviously after HULC silencing.

Conclusion: HULC changed the proteomics characteristics of GBM, including regulating the expression of PLA2G4A. This study provided a new perspective on the menchanisms and potential drug targets of GBM.

Background

GBM is the most common cancer in the central nervous system of adults, characterized by high malignency and aggresiveness [1]. At present, it is treated mainly by surgery, radiotherapy and chemotherapy. Although some new methods of treatment are created, such as photodynamic therapy and immunotherapy, etc [2, 3], their efficacy needs to be further evaluated. Disappointedly, the overall prognosis for GBM patients is poor currently. According to a research in America, the overall survival of GBM patients is about 40.2% for 1 year, and only 5.6% for 5 years [4]. Therefore, it is quite important to deeply explore the menchanisms of GBM and find out suitable biomarkers to help early detective and diagnosis, also to help improve the treatment and prognosis of GBM.

LncRNAs are described as a family of RNA with the length of more than 200 nucleotides, which harbor different functions according to their subcellular localization, primarily involved in gene regulation interecting with other RNAs or proteins, including transcriptional regulation, post-transcriptional regulation and epigenetic regulation, etc [5]. Undoubtedly, increasing evidence shows that lncRNA plays a vital role in tumorigenesis and progression.

HULC was first discovered in liver cancer tissues by Panzitt, et al. revolutionarily [6]. It has attracted huge attention as a result of its most positive regulation, which was the origin of its name. Later it was determined that HULC could promote tumor growth as a form of lncRNA [7]. In addition, several studies have found that HULC is highly expressed in other tumors, such as gastric cancer, colon cancer, ovarian cancer and so on. Related mechanisms are in constant exploration [8–10]. Hong Yan et al. suggested that highly expressed HULC might be utilized as a reference index for the poor prognosis of GBM [11]. However, there is rare study on the mechanisms of how HULC plays a role in GBM till now [12].

Recently, proteomics has been widely used to search for tumor biomarkers [13–15]. MS is the fastest-growing, most dynamic and promising technology in proteomics research. Besides, liquid chromatography mass spectrometry (LC-MS) is considered as an effective tool for the discovery and verification of disease biomarkers due to its high sensitivity, precision, accuracy, and strong quantification capability [16].

The present study detected differentially expressed proteins by taking advantage of highly sensitive quantitative proteomics, combined with bioinformatics analysis to find meaningful targets or signaling pathways involved in pathogenesis between HULC and GBM, which may provide some ideas or directions for targeted therapy of GBM.

Methods

Cell culture

Human glioma cell line U87 was obtained from China Center for Type Culture Collection (Wuhan, China) and cultured with DMEM (BD, Thermo Fisher Scientific, USA) adding 10% FBS (BD, Thermo Fisher Scientific, USA) in a incubator (Thermo Fisher Scientific, USA) containing 5% CO_2 at 37°C.

Construction of transfected stable cell lines

After digested, resuspended and counted, cells were plated on six-well plates at a concentration of 10×10^5 cells per well, and then cultured under the same conditions for 24 hours. Two kinds of 200 ul lentivirus stock solution (GeenPharma, Shanghai, China) after lentiviral packaging and infection was 5 times diluted by DMEM containing 10% FBS. according to the manufacture's protocol. Finally, infection enhancer Polybrene (Sigma□USA) was added to a final concentration of 5 ug/ml. After 96-hour culture, cells were collected at -20°C. So two transfected stable cell lines were constructed, including HULC interference (HULC-siRNA) and its negative control (NC).

QRT-PCR

RNA was extracted from two samples with total RNA extraction kit (QIAGEN, Germany). cDNA was synthesized according to the protocol of high-throughput cDNA reverse transcription kit (Thermo Fisher Scientific, USA). Next, polymerase chain reaction was performed. The relative mRNA levels of target genes were obtained by the $2^{-\Delta\Delta Ct}$ method and determined in triplicate. Upstream sequence of target gene HULC primer: 5'-TCAACCTCCAGAACTGTGATCC-3', down stream sequence: 5'-TGCTTGATGCTTTGGTCTGTT-3'; Upstream sequence of reference gene ACTB primer :5'-CGTGGACATCCGCAAAGA-3', down stream sequence: 5'-GAAGGTGGACAGCGAGGC-3'.

Protein extraction

Samples were sonicated in 4 times volumes of lysis buffer [8 M urea (Sigma, UAS), 1% protease inhibitor (Calbiochem, Germany) and 2 mM EDTA (Sigma□USA)]. The supernatant was collected and the protein concentration was determined with BCA kit (Beyotime, China) according to the manufacture's instructions.

Trypsin digestion

The protein solution was reduced with 5 nM dithiothreitol (Sigma, USA) for 30 minutes at 56°C and incubated in 11 nM iodoacetamide (Sigma, USA) for 15 minutes in the dark at room temperature. Then trypsin (Promega, USA) was added at a ratio of 1:50 trypsin to protein at 37°C overnight and 1:100 for 4 hours.

TMT labeling

The digested peptides were desalted with Strata X C18 SPE column (Phenomenex) and freeze-dried in a vacuum environment. Next they were dissolved in 0.5 M NH_4HCO_3 (Sigma, USA) and labeled with TMT kit (Thermo Fisher Scientific, USA) according to the protocol.

HPLC fractionation

The peptides were fractionated in 8%-32% acetonitrile (Fisher Chemical, USA) under the condition of pH 9 on Agilent 300 Extend C18 column (5 μm size, 4.6 mm inner diameter, 250 mm length) for 60 minutes.

LC-MS/MS analysis

Peptides were dissolved with liquid chromatography mobile phase [aqueous solution contaning 0.1% formic acid (Fluka, USA) and 2% acetonitrile] and seperated on an EASY-nLC 1000 ultra-high performance liquid chromatography system. Later they were injected into the NSI ion source for ionization and

analysis was performed by Orbitrap Fusion Lumos MS. Both the peptide precursor ion and its secondary fragments were detected and analyzed with high-resolution Orbitrap. According to the ratio of mass to charge, they were seperated at the first-stage MS scan. Finally, second-stage separation was performed.

Bioinformatics analysis

Data of second-stage MS was searched in Maxquant (v.1.5.2.8), relevant parameters as showed in Table 1. The quantitative values of each sample were obtained from 3 repeated total proteins quantitative detections. And the relative standard deviation (RSD) was calculated to assess the degree of sample dispersion. Taking the average of 3 quantitative values, fold change was defined as the ratio of 2 averages (HULC-siRNA to NC). The values of log2 fold change were needed to make them consistent with normal distribution and evaluated by two-tailed t-test. Differentially expressed proteins were filtrated based on the following criteria where fold change was more than 1.2 or less than 1/1.2, and P value was less than 0.05 simultaneously. GO annotation of every differentially expressed protein was obtained by searching Uniprot-GOA database or applying Interproscan (v.5.14-53.0), an algorithm software. Moreover, KEGG pathway database (KAAS v.2.0KEGG Mapper v2.5) was utilized to annotate corresponding pathways. The difference in GO enrichment or KEGG pathway enrichment was further evaluated by two-tailed Fisher's exact test (Perl module v.1.31), where corrected P value <0.05 was considered statistically different.

Table 1
Relevant parameters for Maxquant database searching

Parameter		Value
Protein database		SwissProt Human (20317 sequences)
Cleavage enzyme		Trypsin/P
Missing cleavages		2
Minimum length of peptide		7 amino acid residues
Maximum modifications of peptide		5
Mass tolerance for precursor ions	First search	20 ppm
	Main search	5 ppm
Mass tolerance for fragment ions		0.02 Da
Fixed modification		Carbamidomethyl on Cys
Variable modification		oxidation on Met, N-terminal acetylation
Quantitative method		TMT-6plex
FDR for protein identification		1%
FDR for PSM identification		1%

Results

The detection of expression of HULC in two stable cell lines by qRT-PCR

The relative expression of HULC in NC was 1.05±0.101, and 0.680±0.0890 in HULC-siRNA (t=4.82 P=0.00860). So it was clear that the relative expression of HULC in HULC-siRNA was significantly lower than it in NC (Fig. 1A), which illustrated the successful construction of stable cell lines.

Statistics of differentially expressed proteins

Since the overall RSD values of two sample groups were pretty small, protein samples obtained from LC-MS/MS analysis harbored high repeatability and quality (Fig. 1B). Quantitative values of proteins in HULC-siRNA were compared with those in NC. When P value < 0.05, fold change > 1.2 was regarded as up regulation. Conversely, fold change < 1/1.2 was regarded as down regulation. A total of 112 up-regulated proteins and 24 down-regulated proteins were detected (Table 2). Then the volcano plot was made with log2 fold change as the abscissa, and -log10 P value as the ordinate (Fig. 1C).

Table 2
An overview of differentially expressed proteins

Protein accession	Protein description	Gene name	MW[kDa]	siRNA/NC ratio
P0C7I6	Coiled-coil domain-containing protein 159	CCDC159	33.695	2.267
O94885	SAM and SH3 domain-containing protein 1	SASH1	136.65	1.523
Q5VT79	Annexin A8-like protein 1	ANXA8L1	36.879	1.506
P47712	Cytosolic phospholipase A2	PLA2G4A	85.238	1.458
Q16850	Lanosterol 14-alpha demethylase	CYP51A1	56.805	1.347
Q6ZMG9	Ceramide synthase 6	CERS6	44.889	1.336
Q12872	Splicing factor, suppressor of white-apricot homolog	SFSWAP	104.82	1.313
P05109	Protein S100-A8	S100A8	10.834	1.3
P13521	Secretogranin-2	SCG2	70.94	1.292
P07451	Carbonic anhydrase 3	CA3	29.557	1.292
O60218	Aldo-keto reductase family 1 member B10	AKR1B10	36.019	1.289
P23219	Prostaglandin G/H synthase 1	PTGS1	68.686	1.267
Q9Y5U8	Mitochondrial pyruvate carrier 1	MPC1	12.347	1.266
Q9NZA1	Chloride intracellular channel protein 5	CLIC5	46.502	1.257
Q9ULF5	Zinc transporter ZIP10	SLC39A10	94.131	1.255
Q9BWD1	Acetyl-CoA acetyltransferase, cytosolic	ACAT2	41.35	1.237
P48735	Isocitrate dehydrogenase [NADP], mitochondrial	IDH2	50.909	1.228
P53602	Diphosphomevalonate decarboxylase	MVD	43.404	1.227
Q9H900	Protein zwilch homolog	ZWILCH	67.213	1.224
P18827	Syndecan-1	SDC1	32.461	1.22
Q969H8	Myeloid-derived growth factor	MYDGF	18.795	1.213

Protein accession	Protein description	Gene name	MW[kDa]	siRNA/NC ratio
Q6NYC1	Bifunctional arginine demethylase and lysyl-hydroxylaseJMJD6	JMJD6	46.461	1.209
P06703	Protein S100-A6	S100A6	10.18	1.207
P61586	Transforming protein RhoA	RHOA	21.768	1.201
Q9Y2B9	cAMP-dependent protein kinase inhibitor gamma	PKIG	7.9104	0.832
Q5VIR6	Vacuolar protein sorting-associated protein 53 homolog	VPS53	79.652	0.831
O95319	CUGBP Elav-like family member 2	CELF2	54.284	0.83
P22626	Heterogeneous nuclear ribonucleoproteins A2/B1	HNRNPA2B1	37.429	0.83
Q86V81	THO complex subunit 4	ALYREF	26.888	0.83
Q8WV24	Pleckstrin homology-like domain family A member 1	PHLDA1	45.016	0.83
P54792	Putative segment polarity protein dishevelled homolog DVL1P1	DVL1P1	73.253	0.829
Q9Y5J5	Pleckstrin homology-like domain family A member 3	PHLDA3	13.891	0.829
P62244	40S ribosomal protein S15a	RPS15A	14.839	0.828
P17480	Nucleolar transcription factor 1	UBTF	89.405	0.828
Q8N684	Cleavage and polyadenylation specificity factor subunit 7	CPSF7	52.049	0.827
Q14195	Dihydropyrimidinase-related protein 3	DPYSL3	61.963	0.827
P45973	Chromobox protein homolog 5	CBX5	22.225	0.827
Q9UBS8	E3 ubiquitin-protein ligase RNF14	RNF14	53.837	0.827
P23246	Splicing factor, proline- and glutamine-rich	SFPQ	76.149	0.827
O15061	Synemin	SYNM	172.77	0.825
P19338	Nucleolin	NCL	76.613	0.825
Q8NCN5	Pyruvate dehydrogenase phosphatase regulatory subunit, mitochondrial	PDPR	99.363	0.823

Protein accession	Protein description	Gene name	MW[kDa]	siRNA/NC ratio
O60315	Zinc finger E-box-binding homeobox 2	ZEB2	136.45	0.823
P57723	Poly(rC)-binding protein 4	PCBP4	41.481	0.823
P09471	Guanine nucleotide-binding protein G(o) subunit alpha	GNAO1	40.05	0.822
Q9P2 × 3	Protein IMPACT	IMPACT	36.476	0.82
Q9Y2E5	Epididymis-specific alpha-mannosidase	MAN2B2	113.98	0.82
Q96L93	Kinesin-like protein KIF16B	KIF16B	152.01	0.82
Q6ICG6	Uncharacterized protein KIAA0930	KIAA0930	45.794	0.819
Q9Y3Y2	Chromatin target of PRMT1 protein	CHTOP	26.396	0.819
P50579	Methionine aminopeptidase 2	METAP2	52.891	0.819
Q13509	Tubulin beta-3 chain	TUBB3	50.432	0.818
P16403	Histone H1.2	HIST1H1C	21.364	0.817
O75914	Serine/threonine-protein kinase	PAK3	62.309	0.816
Q14938	Nuclear factor 1 X-type	NFIX	55.098	0.814
Q9BQ89	Protein FAM110A	FAM110A	31.27	0.811
Q9Y6R0	Numb-like protein	NUMBL	64.891	0.81
Q6WCQ1	Myosin phosphatase Rho-interacting protein	MPRIP	116.53	0.81
P08138	Tumor necrosis factor receptor superfamily member 16	NGFR	45.183	0.808
Q05682	Caldesmon	CALD1	93.23	0.808
Q9P2K5	Myelin expression factor 2	MYEF2	64.121	0.808
Q92556	Engulfment and cell motility protein 1	ELMO1	83.829	0.808
Q9UPQ7	E3 ubiquitin-protein ligase PDZRN3	PDZRN3	119.6	0.807
Q96T51	RUN and FYVE domain-containing protein 1	RUFY1	79.817	0.807
P39019	40S ribosomal protein S19	RPS19	16.06	0.805
Q01130	Serine/arginine-rich splicing factor 2	SRSF2	25.476	0.805
Q6DN90	IQ motif and SEC7 domain-containing protein 1	IQSEC1	108.31	0.804

Protein accession	Protein description	Gene name	MW[kDa]	siRNA/NC ratio
Q9Y2D5	A-kinase anchor protein 2	AKAP2	94.659	0.803
Q13557	Calcium/calmodulin-dependent protein kinase type II subunit delta	CAMK2D	56.369	0.803
Q6GYQ0	Ral GTPase-activating protein subunit alpha-1	RALGAPA1	229.83	0.801
Q9Y3E1	Hepatoma-derived growth factor-related protein 3	HDGFL3	22.619	0.801
Q9Y4J8	Dystrobrevin alpha	DTNA	83.9	0.8
Q8IWA4	Mitofusin-1	MFN1	84.159	0.8
Q9H2L5	Ras association domain-containing protein 4	RASSF4	36.748	0.798
P53999	Activated RNA polymerase II transcriptional coactivator p15	SUB1	14.395	0.797
Q15052	Rho guanine nucleotide exchange factor 6	ARHGEF6	87.498	0.796
O43281	Embryonal Fyn-associated substrate	EFS	58.815	0.795
Q9BVA1	Tubulin beta-2B chain	TUBB2B	49.953	0.795
Q9UHB6	LIM domain and actin-binding protein 1	LIMA1	85.225	0.794
P42262	Glutamate receptor 2	GRIA2	98.82	0.792
Q15233	Non-POU domain-containing octamer-binding protein	NONO	54.231	0.792
P00966	Argininosuccinate synthase	ASS1	46.53	0.792
Q9NYF8	Bcl-2-associated transcription factor 1	BCLAF1	106.12	0.791
P62888	60S ribosomal protein L30	RPL30	12.784	0.791
O43707	Alpha-actinin-4	ACTN4	104.85	0.79
Q15018	BRISC complex subunit Abraxas 2	ABRAXAS2	46.9	0.79
P11532	Dystrophin	DMD	426.74	0.789
Q96KR1	Zinc finger RNA-binding protein	ZFR	117.01	0.788
Q6NZI2	Caveolae-associated protein 1	CAVIN1	43.476	0.787

Protein accession	Protein description	Gene name	MW[kDa]	siRNA/NC ratio
Q5M775	Cytospin-B	SPECC1	118.58	0.787
O00159	Unconventional myosin-Ic	MYO1C	121.68	0.785
P12814	Alpha-actinin-1	ACTN1	103.06	0.784
P35579	Myosin-9	MYH9	226.53	0.782
P49006	MARCKS-related protein	MARCKSL1	19.529	0.777
P29972	Aquaporin-1	AQP1	28.526	0.775
Q7RTV2	Glutathione S-transferase A5	GSTA5	25.722	0.773
Q9NQS1	Cell death regulator Aven	AVEN	38.506	0.772
O15075	Serine/threonine-protein kinase DCLK1	DCLK1	82.223	0.769
P07305	Histone H1.0	H1F0	20.863	0.767
Q92804	TATA-binding protein-associated factor 2N	TAF15	61.829	0.766
Q14978	Nucleolar and coiled-body phosphoprotein 1	NOLC1	73.602	0.761
Q9H936	Mitochondrial glutamate carrier 1	SLC25A22	34.47	0.759
Q8IWT1	Sodium channel subunit beta-4	SCN4B	24.969	0.756
Q8WWI5	Choline transporter-like protein 1	SLC44A1	73.301	0.753
Q32NB8	CDP-diacylglycerol–glycerol-3-phosphate 3-phosphatidyltransferase, mitochondrial	PGS1	62.73	0.753
Q96CT7	Coiled-coil domain-containing protein 124	CCDC124	25.835	0.75
Q9BX67	Junctional adhesion molecule C	JAM3	35.02	0.747
O94875	Sorbin and SH3 domain-containing protein 2	SORBS2	124.11	0.747
Q9UKA9	Polypyrimidine tract-binding protein 2	PTBP2	57.49	0.747
Q14011	Cold-inducible RNA-binding protein	CIRBP	18.648	0.744
Q14123	Calcium/calmodulin-dependent 3',5'-cyclic nucleotide phosphodiesterase 1C	PDE1C	80.759	0.74
Q7Z406	Myosin-14	MYH14	227.87	0.739

Protein accession	Protein description	Gene name	MW[kDa]	siRNA/NC ratio
Q14315	Filamin-C	FLNC	291.02	0.738
Q08945	FACT complex subunit SSRP1	SSRP1	81.074	0.737
Q16643	Drebrin	DBN1	71.428	0.735
Q96C19	EF-hand domain-containing protein D2	EFHD2	26.697	0.735
P48681	Nestin	NES	177.44	0.728
Q99715	Collagen alpha-1(XII) chain	COL12A1	333.14	0.727
P21589	5'-nucleotidase	NT5E	63.367	0.703
P08670	Vimentin	VIM	53.651	0.699
O75882	Attractin	ATRN	158.54	0.698
P30838	Aldehyde dehydrogenase, dimeric NADP-preferring	ALDH3A1	50.394	0.693
P27658	Collagen alpha-1(VIII) chain	COL8A1	73.363	0.693
P04114	Apolipoprotein B-100	APOB	515.6	0.685
P02794	Ferritin heavy chain	FTH1	21.225	0.681
Q6ZN11	Zinc finger protein 793	ZNF793	46.926	0.665
Q8N3V7	Synaptopodin	SYNPO	99.462	0.664
P09493	Tropomyosin alpha-1 chain	TPM1	32.708	0.636
Q6RFH5	WD repeat-containing protein 74	WDR74	42.441	0.62
Q01995	Transgelin	TAGLN	22.611	0.609
Q8TAC9	Secretory carrier-associated membrane protein 5	SCAMP5	26.104	0.606
Q9UBF6	RING-box protein 2	RNF7	12.683	0.586
P02511	Alpha-crystallin B chain	CRYAB	20.159	0.581
P25189	Myelin protein P0	MPZ	27.554	0.567
Q8IYE0	Coiled-coil domain-containing protein 146	CCDC146	112.81	0.514
P02656	Apolipoprotein C-III	APOC3	10.852	0.5

GO annotation and enrichment

GO annotation is classified into 3 categories (biological process, cellular component, molecular function) to explain the biological role of each protein from different perspectives. Two charts illustrated the distribution of differentially expressed proteins in GO terms level 2 (Fig. 1D and 1E). Taken together, it was clear that dysregulated proteins were mainly involved in cellular or single-organism process and biological regulation under the classification of biological process, making up cell and organelle under the classification of cellular component. And as for molecular function, they were concentrated on binding and catalytic activity. Moreover, Fisher's exact test was applied to perform GO enrichment analysis. Directed acyclic graphs reflected not only the enrichment difference of GO classification, but also the hierarchical relationship intuitively. It could be concluded that significantly different GO classifications were mostly enriched in binding, metabolism, regulation, and catalytic functions. And they were also enriched at deeper and more detailed levels of grade (Fig. 2 and 3).

KEGG pathway annotation and enrichment

All differentially expressed proteins were annotated with KEGG pathway. Furthermore, in order to reflect whether there was any significant enrichment trend of those proteins in annotated KEGG pathways, the enrichment test was performed with Fisher's exact test and P values were presented as -log10 conversion. It was exhibited that tight junction was most enriched in up-regulated pathways after the interference of HULC, while down-regulated KEGG pathways preferred metabolic pathway, arachidonic acid metabolism, terpenoid backbone biosynthesis and platelet activation (Fig. 3).

Discussion

GBM is the fourth grade of glioma with the highest malignancy. Increasing evidence demonstrates the dysregulation of many kinds of lncRNAs is involved in a series of biological processes in the occurrence and development of GBM. For example, highly expressed PVT1 could improve the proliferation, invasion and aerobic glycolysis in glioma cell by inhibiting the expression of miR-140-5p [17]. Another lncRNA GAS5-AS1 could bind miR-106b-5p to promote the expression of downstream genes and thus play a role in inhibiting the proliferation, migration and invasion of glioma [18]. Studies are emerging quickly on the mechanisms of how lncRNA influence other tumors [19,20], aimed to search for highly specific and sensitive biomarkers to help make early diagnosis, predict prognosis, and provide potential therapeutic targets of cancers.

LncRNA HULC has been proved to harbor a significantly higher level in GBM cells than normal cells, and promote the proliferation of GBM in vitro [11]. Yu Zhu et al. have found that HULC silencing could inhibit angiogenesis of glioma through ESM-1 mediated PI3K/AKT/mTOR signaling pathway, resulting in the suppression of GBM growth [12].

Proteomics research is currently in full swing. Islam Farhadul et al. studied and analyzed the differences of total proteome between esophageal squamous cell carcinoma and non-tumor cell through quantitative

proteomics based on MS [13]. Qingchuan zhao et al. screened tumor-specific antigens for high-grade serous ovarian cancer with MS, which might become suitable targets for ovarian cancer immunotherapy [14]. In this study, we have obtained the proteome of HULC-siRNA and NC through TMT labeling, HPLC fractionation technology and LC-MS/MS analysis, hoping excavate some promising biomarkers.

Among all differentially expressed proteins, the top 5 of up regulation or down regulation were analyzed in detail respectively. In PubMed database, none of the above 10 proteins were reported to be related to HULC. However, there have been some studies between CRYAB or SASH1 and glioma [21,22]. No related reports have been found on the remaining 8 proteins associated with glioma till now. And other proteins were not analyzed this time. Undoubtedly, deeper learning of these proteins is helpful for further study in molecular mechanisms.

GO database is applied to describe various properties of genes and gene products. GO annotation demonstrated that differentially expressed proteins were primarily involved in cellular biological processes and constituting cell and organelle structures. More importantly, they played a role in molecular binding and catalytic activities. The above could make some influence to the proliferation, migration of GBM, which undoubtedly reflected the crucial influence of HULC on GBM. The trend of GO enrichment was consistent with the results of secondary GO classification. In addition, it explained some crucial processes of how HULC microscopically regulated GBM in depth, such as calcium-dependent phospholipid binding, methylase activity, regulation of angiogenesis and so on. As we all know, DNA methylation is an early event of tumorigeneisis. For example, the methylation level of the MGMT promoter in gliomas might be associated with prognosis and recurrence [23]. Moreover, the methylation of SASH1 was conducive to weakening cell adhesion [22]. Thus it was considered that the methylation of HULC could be put into following study.

KEGG is an information network describing the interactions between known molecules, such as information transmission, protein-protein interaction, and biochemical reactions. KEGG pathway mostly includes metabolism, cell growth, genetic or environmental information processing, human diseases, drug development and so on. In the present study, it was revealed that tight junction had a strongest enrichment under the up-regulated pathways, which further implied that the interference of HULC could improve cell adhesion and suppress migration of GBM. At the same time, terpenoid backbone biosynthesis presented obvious difference in down-regulated pathways, indicating that HULC silencing might act on inhibiting cell proliferation. In addition, down-regulated pathway of platelet activation prompted that HULC was related to the complication of GBM like thrombosis to some extent.

Comparing some down-regulated pathways (arachidonic acid metabolism, platelet activation), we have found that cPLA2α was one of the common proteins and might act as a crucial role. cPLA2α, encoded by PLA2G4A gene, is the most abundant subtype in the family of phospholipase A2. Phospholipase can hydrolyze membrane phospholipids to arachidonic acid, which is further involved in many Pathological and physiological processes, including inducing inflammation, transmitting signals, and promoting cell growth, etc. Although one study has shown that down expression of PLA2G4A can promote the migration

and invasion of esophageal squamous cell carcinoma [24], most researchers considered that PLA2G4A was an oncogene [25-27], which was consistent with our results. The data showed that the expression level of PLA2G4A notably decrease after HULC silencing. Thus, it was suspected that PLA2G4A was likely to be one of the key point of how HULC acted on GBM, which also echoed arachidonic acid metabolism, the most significant pathway in down-regulated category. Since the concept of tumor-promoting inflammation was proposed in 2011 [28], tumor-associated chronic inflammation is a key trigger point for cancer progression, we can assume that the inflammation induced by arachidonic acid metabolism pathway is an important participant in the development of GBM. Undoubtedly, more specific mechanisms need further verification and research.

Conclusions

- We concluded that HULC had changed the proteomics characteristics of GBM. And PLA2G4A was prominantly regulated by HULC in GBM cells. This study provided a new perspective on the pathogenesis of GBM, and a starting point of GBM targeted therapy. Nevertheless, the number of differentially expressed proteins detected this time was relatively small, which stimulated more research for quantitative proteome assay on cell models or tissues of over-expressive HULC.

Abbreviations

GBM: glioblastoma multiforme

HULC: highly up-regulated in liver cancer

siRNA: small interfering RNA

MS: mass spectrometry

GO: gene ontology

KEGG: Kyoto Encyclopedia of Genes and Genomes

LC-MS: liquid chromatography mass spectrometry

TMT: Tandem Mass Tags

HPLC: high performance liquid chromatography

Declarations

Acknowledgements

Not applicable.

Authors' contributions

JH put forward the idea and study design. SY performed the research conceptualization and data curation. YW and TYwas responsible for the data searching and analysis. SY and YH applied all results and prepared charts. SY wrote the first draft of the manuscript. All authors read and approved the final manuscript.

Funding

The present study was supported by the National Natural Science Foundation of China (no. 81872055).

Availability of data and materials

The datasets analysed during the current study are available from the corresponding author on reasonable request.

Ethics approval and consent to participate

Not applicable.

Consent for publication

Not applicable.

Competing interests

The authors declare that they have no competing interests.

References

1. Thakkar JP, et al. Epidemiologic and molecular prognostic review of glioblastoma. Cancer Epidem Biomar. 2014;23(10):1985–96.
2. Youssef Z, et al. New targeted gold nanorods for the treatment of glioblastoma by photodynamic therapy. J Clin Med. 2019;8(12):2205.
3. Polivka J Jr, et al. Advances in experimental targeted therapy and immunotherapy for patients with glioblastoma multiforme. Anticancer Res. 2017;37(1):21–33.
4. Ostrom QT, et al. CBTRUS statistical report: primary brain and other central nervous system tumors diagnosed in the United States in 2011–2015. Neuro Oncol. 2018;20(suppl_4):iv1–86.
5. Chen LL. Linking long noncoding RNA localization and function. Trends Biochem Sci. 2016;41(9):761–72.
6. Panzitt K, et al. Characterization of HULC, a novel gene with striking up-regulation in hepatocellular carcinoma, as noncoding RNA. Gastroenterology. 2007;132(1):330–42.

7. Xiong H, et al. LncRNA HULC promotes the growth of hepatocellular carcinoma cells via stabilizing COX-2 protein. Biochem Biophys Res Commun. 2017;490(3):693–9.
8. Liu T, et al. LncRNA HULC promotes the progression of gastric cancer by regulating miR-9-5p/MYH9 axis. Biomed Pharmacother. 2020;121:109607.
9. Dong Y, et al. Long non-coding RNA HULC interacts with miR-613 to regulate colon cancer growth and metastasis through targeting RTKN. Biomed Pharmacother. 2019;109:2035–42.
10. Chu P, Xu LN, Su HY. HULC functions as an oncogene in ovarian carcinoma cells by negatively modulating miR-125a-3p. J Physiol Biochem. 2019;75(2):163–71.
11. Yan H, et al. High expression of long noncoding RNA HULC is a poor predictor of prognosis and regulates cell proliferation in glioma. Onco Targets Ther. 2016;10:113–20.
12. Zhu Y, et al. HULC long noncoding RNA silencing suppresses angiogenesis by regulating ESM-1 via the PI3K/Akt/mTOR signaling pathway in human gliomas. Oncotarget. 2016;7(12):14429–40.
13. Islam F, Gopalan V, Lam AK. Mass spectrometry for biomarkers discovery in esophageal squamous cell carcinoma. Methods Mol Biol. 2020;2129:259–68.
14. Zhao Q, et al. Proteogenomics uncovers a vast repertoire of shared tumor-specific antigens in ovarian cancer. Cancer Immunol Res. 2020;8(4):544–55.
15. Deb B, et al. Bioinformatics analysis of global proteomic and phosphoproteomic data sets revealed activation of NEK2 and AURKA in cancers. Biomolecules. 2020;10(2):237.
16. Li HL, et al. Assessing the utility of multiplexed liquid chromatography-mass spectrometry for gluten detection in australian breakfast food products. Molecules. 2019;24(20):3665.
17. Shao Y, et al. Long non-coding RNA PVT1 regulates glioma proliferation, invasion, and aerobic glycolysis via miR-140-5p. Eur Rev Med Pharmacol Sci. 2020;24(1):274–83.
18. Huang W, et al. LncRNA GAS5-AS1 inhibits glioma proliferation, migration, and invasion via miR-106b-5p/TUSC2 axis. Hum Cell. 2020;33(2):416–26.
19. Zhang Q, et al. Comprehensive analysis of the long noncoding RNA expression profile and construction of the lncRNA-mRNA co-expression network in colorectal cancer. Cancer Biol Ther. 2020;21(2):157–69.
20. Cao YP, et al. Long non-coding RNA in bladder cancer. Clin Chim Acta. 2020;503:113–21.
21. Kore RA, Abraham EC. Phosphorylation negatively regulates exosome mediated secretion of cryAB in glioma cells. Biochim Biophys Acta. 2016;1863(2):368–77.
22. Wu R, et al. HMGB1 contributes to SASH1 methylation to attenuate astrocyte adhesion. Cell Death Dis. 2019;10(6):417.
23. Mathur R, et al. MGMT promoter methylation level in newly diagnosed low-grade glioma is a predictor of hypermutation at recurrence. Neuro Oncol. 2020. doi:10.1093/neuonc/noaa059.
24. Zhao HY, et al. MiR-543 promotes migration, invasion and epithelial-mesenchymal transition of esophageal cancer cells by targeting phospholipase A2 group IVA. Cell Physiol Biochem. 2018;48(4):1595–604.

25. Bai HS, et al. PLA2G4A is a potential biomarker predicting shorter overall survival in patients with non-M3/NPM1 wildtype acute myeloid leukemia. DNA Cell Biol. 2020;39(4):700–8.
26. Tunset HM, et al. Cytosolic phospholipase A2 alpha regulates TLR signaling and migration in metastatic 4T1 cells. Int J Mol Sci. 2019;20(19):4800.
27. Pang X, et al. cPLA2a correlates with metastasis and poor prognosis of osteosarcoma by facilitating epithelial-mesenchymal transition. Pathol Res Pract. 2019;215(6):152398.
28. Hanahan D, Weinberg RA. Hallmarks of cancer: the next generation. Cell. 2011;144(5):646–74.

Figures

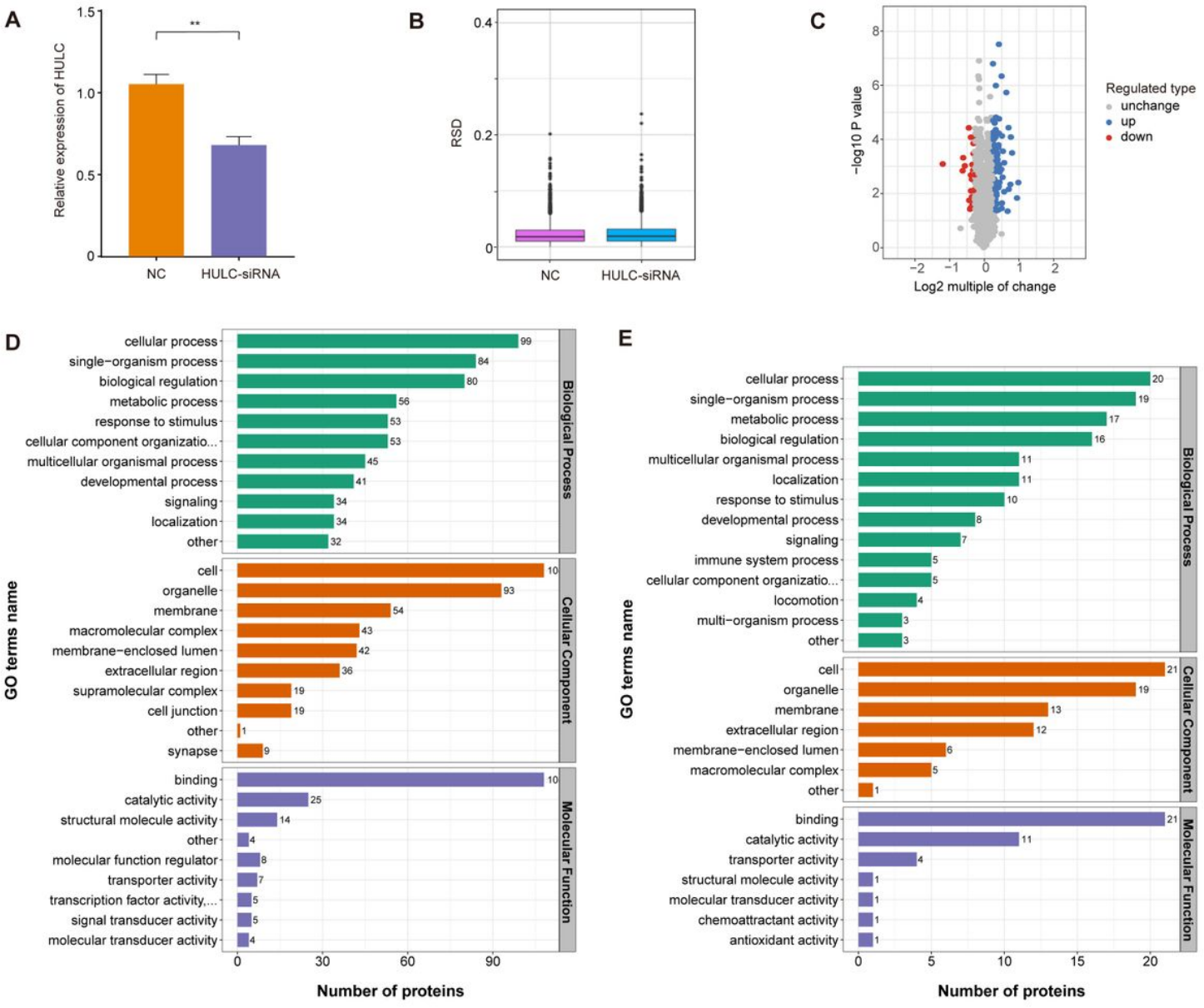

Figure 1

A qRT-PCR was operated in U87 stable cell lines to illustrate that the relative expression level of HULC in HULC-siRNA was significantly lower than it in NC(t=4.815,P=0.00860,**P<0.01). B The box plot of RSD revealed good repeatability among all quantified proteins. C The volcano plot elucidated the comparison of differentially expressed protein between NC and HULC-siRNA performed by liquid chromatography mass spectrometry/mass spectrometry. D The chart demonstrated how up-regulated proteins were distributed in biological process, cellular component and molecular function respectively. E All down-regulated proteins were classified under GO terms level 2.

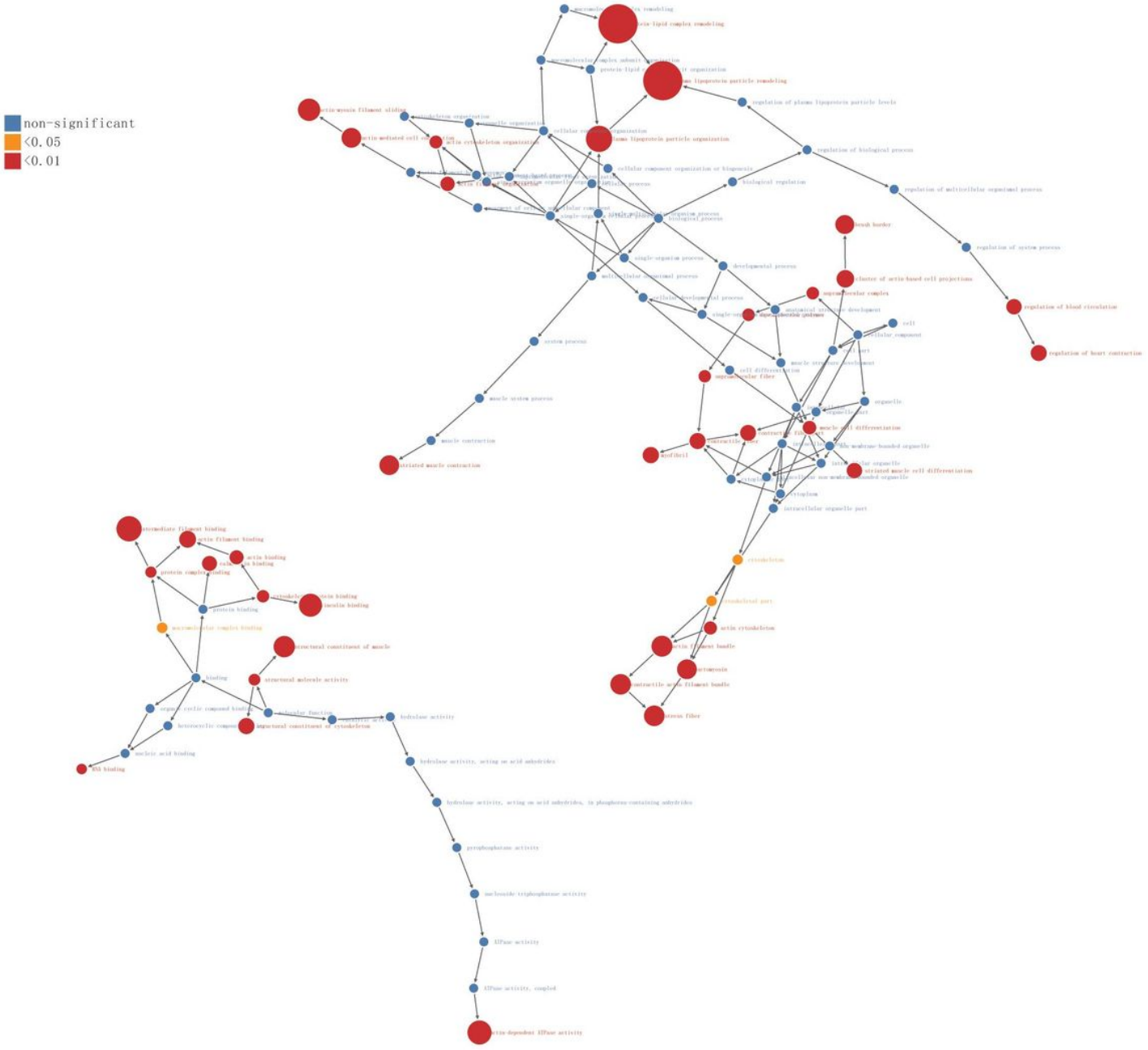

Figure 2

The GO enrichment of up-regulated proteins were analyzed by Fisher's exact test, which presented the obvious enrichment in binding, metabolism, regulation, and catalytic functions.

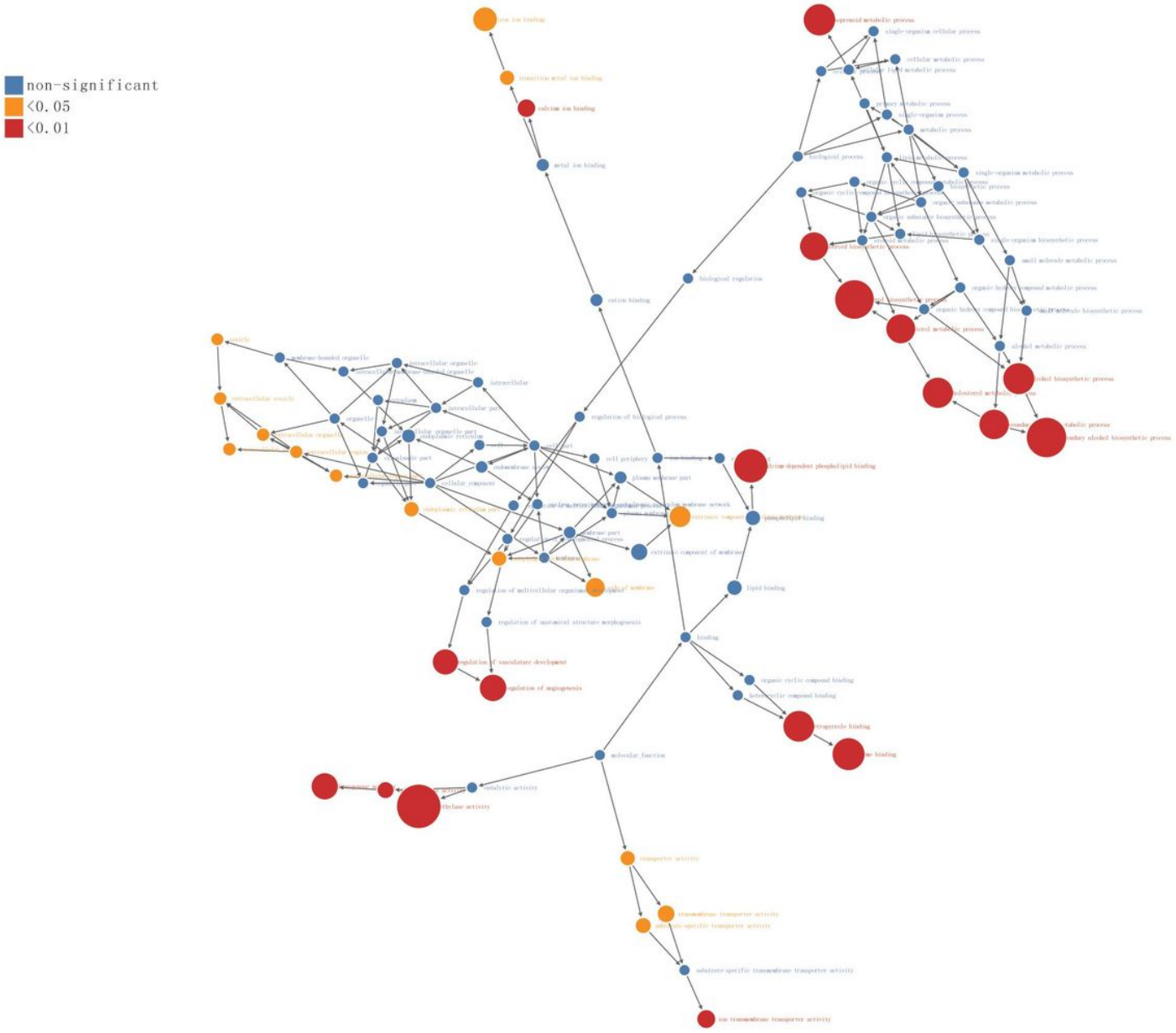

Figure 3

The GO enrichment of down-regulated proteins was similar as up-regulated proteins at deeper and more detailed levels of grade.

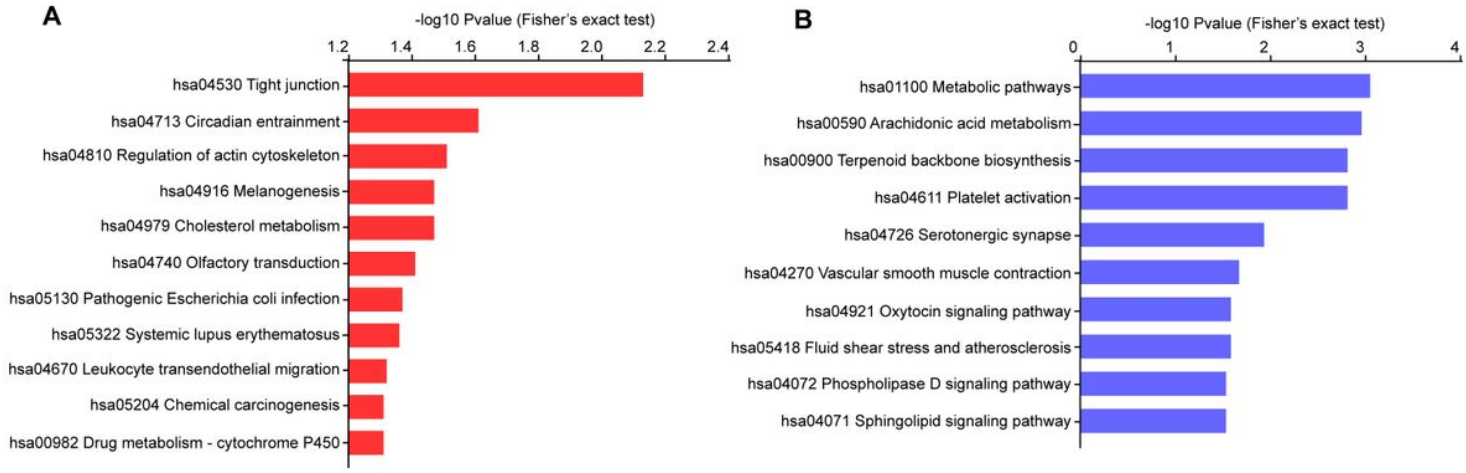

Figure 4

A KEGG pathway enrichment of up-regulated proteins were performed by Fisher's exact test, which illustrated tight junction was most enriched. B The plot exhibited 10 down-regulated KEGG pathways with significant enrichment.